The Company of Biologists

RESEARCH REPORT

Stochastic single cell migration leads to robust horizontal cell layer formation in the vertebrate retina

Rana Amini*, Anastasia A. Labudina and Caren Norden*

ABSTRACT

Developmental programs that arrange cells and tissues into patterned organs are remarkably robust. In the developing vertebrate retina, for example, neurons reproducibly assemble into distinct layers giving the mature organ its overall structured appearance. This stereotypic neuronal arrangement, termed lamination, is important for efficient neuronal connectivity. Although retinal lamination is conserved in many vertebrates, including humans, how it emerges from single cell behaviour is not fully understood. To shed light on this issue, we here investigated the formation of the retinal horizontal cell layer. Using *in vivo* light sheet imaging of the developing zebrafish retina, we generated a comprehensive quantitative analysis of horizontal single cell behaviour from birth to final positioning. Interestingly, we find that all parameters analysed, including cell cycle dynamics, migration paths and kinetics, as well as sister cell dispersal, are very heterogeneous. Thus, horizontal cells show individual non-stereotypic behaviour before final positioning. Yet these initially variable cell dynamics always generate the correct laminar pattern. Consequently, our data show that the extent of single cell stochasticity in the lamination of the vertebrate retina is underexplored.

KEY WORDS: Retina, Horizontal cells, Migration and lamination, Stochastic single cell migration, Zebrafish

INTRODUCTION

During development, tissues and organs change their morphology to acquire the characteristic sizes, shapes and cellular patterns that ensure correct function. These processes are tightly regulated to yield reproducible outcomes and precise tissue patterning. The vertebrate retina is a fascinating example of such pattern formation. As an extension of the central nervous system, it develops from a pool of multipotent progenitors into a neural tissue composed of five neuronal cell types. Neurons of the same type, as well as the one glial cell type, Müller glia, are positioned in distinct layers that give the mature retina its laminated appearance (Fig. 1A). Interestingly, retinal development contains stochastic elements. For example, stochasticity in the apical-basal movement of neuroepithelial cell nuclei has been proposed to contribute to proliferative versus neurogenic division outcome in zebrafish (Baye and Link, 2007; Del Bene et al., 2008). In addition, stochasticity has been suggested to be involved in retinal neuronal fate determination (He et al., 2012). Studies so far have concentrated on exploring stochasticity of fate decisions; however, to

Max Planck Institute of Molecular Cell Biology and Genetics, Pfotenhauerstraße 108, 01307 Dresden, Germany.

*Authors for correspondence (norden@mpi-cbg.de; amini@mpi-cbg.de)

R.A., 0000-0002-3974-5072; A.A.L., 0000-0002-5544-5627; C.N., 0000-0001-8835-1451

what extent other phenomena, particularly retinal lamination, also show variability or stochastic elements remains unknown. To address this issue, we explored single cell behaviour of horizontal cells (HCs) before lamination. HCs are inhibitory interneurons that localize beneath the photoreceptor (PR) cell layer and form synaptic connections with PRs and bipolar cells (BCs) (Amini et al., 2018). BCs ultimately transmit visual information to the retinal ganglion cells (RGCs) (Fig. 1A). Committed HC precursors (HCpr) divide once more before integrating into their laminar array, producing two HCs (Godinho et al., 2007; Weber et al., 2014). The timing and dynamics of this last cell cycle have not yet been studied. Furthermore, HC migration patterns are not fully understood. Unlike RGCs, which keep an apical connection and reach their final destination via stereotypic somal translocation (Icha et al., 2016), HCs are not attached but instead undergo multipolar bidirectional migration to reach their final position (Chow et al., 2015; Edqvist and Hallböök, 2004). Although different phases of movement have been characterized (Chow et al., 2015), the stereotypicity of these movements remains unexplored.

Here, we use long-term *in vivo* light sheet imaging to quantify single cell behaviour over a large cohort of HCs following cell-cycle parameters and bidirectional migration (Chow et al., 2015; Godinho et al., 2007; Weber et al., 2014). Surprisingly, we find that cell cycle parameters substantially vary among single cells and that migration patterns of single cells are non-predictable before robust final lamination. Thus, we provide the first evidence that, as seen for fate decisions, retinal lamination also contains variable and stochastic elements.

RESULTS

HCprs vary in mitotic position, mitotic length and spindle orientation

Before final lamination, committed HCprs undergo one more division. The position of this division is not restricted to the final HC location but can occur along the inner nuclear layer (INL) (Godinho et al., 2007; Weber et al., 2014). As previous studies used immunostaining of fixed samples, no appreciation of HCpr division dynamics existed so far.

Following 428 cells from 21 embryos (i.e. $n=428$, $N=21$) (for an experimental example see Movie 1 and Fig. 1B), we found that, as postulated previously (Godinho et al., 2007; Weber et al., 2014), all HCprs underwent an additional division resulting in two HCs that later entered the HC layer (data from all pooled movies, Table S3). None of the tracked HCprs underwent more than one terminal division (data from all pooled movies Table S3). Single cell analysis of mitotic location (Fig. 1D,D′) ($n=428$, $N=21$) revealed variations in HCpr mitotic position. Although most cells entered and underwent mitosis near the outer plexiform layer (OPL) where they later resided, divisions were also seen along the whole apico-basal length of the INL, even close to the inner plexiform layer (IPL) (Fig. 1C-E). All markers used (see Material and Methods) showed a
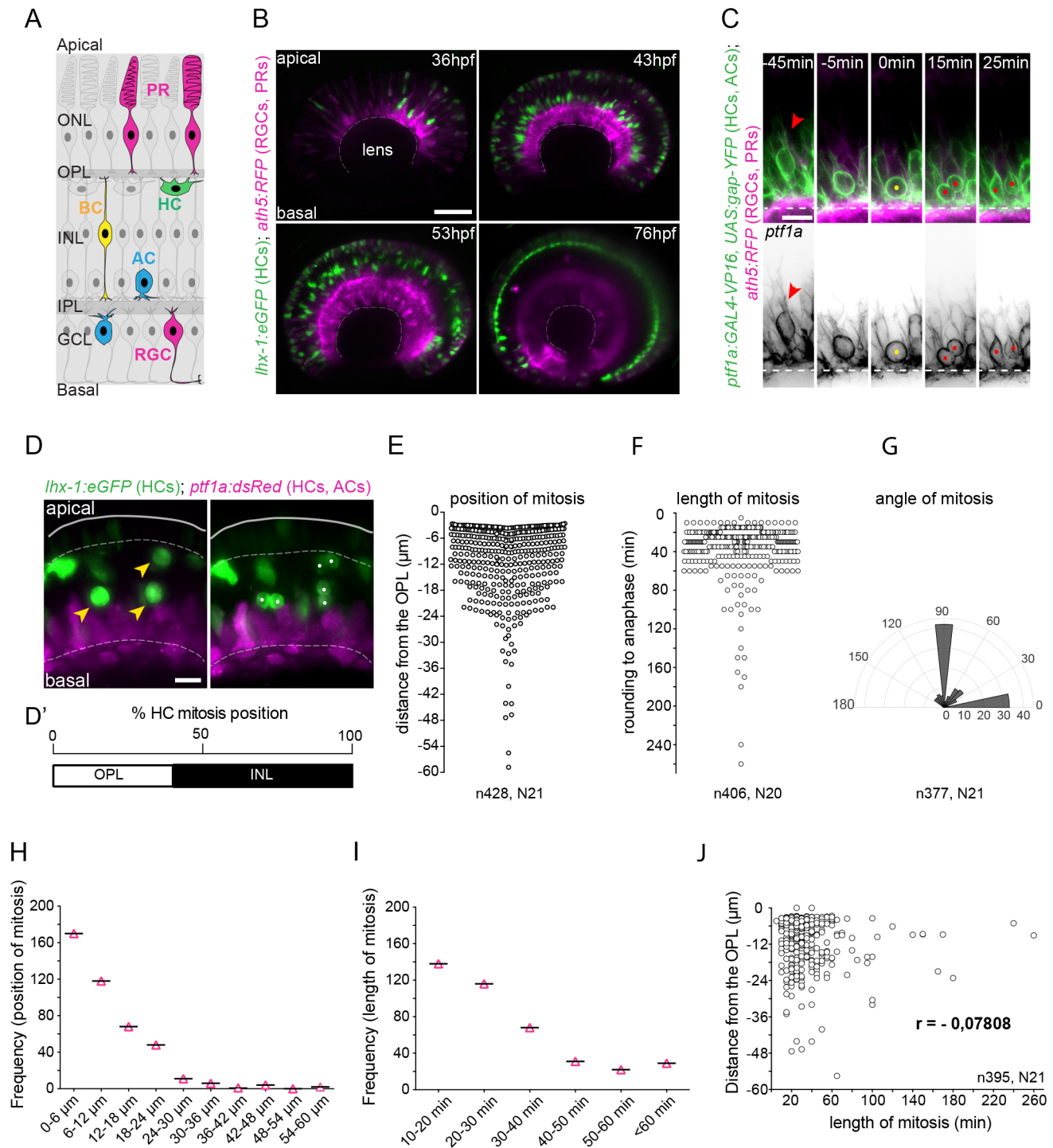
Fig. 1. Heterogeneity in mitotic position and behaviour of HCprs. (A) Scheme of zebrafish retina. Neurons: photoreceptors (PRs, magenta); horizontal cells (HCs, green); bipolar cells (BCs, yellow); amacrine cells (ACs, blue) and retinal ganglion cells (RGCs, magenta). Layers: outer nuclear layer (ONL), inner nuclear layer (INL), ganglion cell layer (GCL), outer plexiform layer (OPL) and inner plexiform layer (IPL). (B) Montage of HC lamination 36 hpf-76 hpf. *lhx-1:eGFP* (HC and PR, green), *ptf1a:dsRed* (AC and HC, magenta). Scale bar: 10 μm. (C) Montage representing a typical example of HCpr mitosis length. Time is relative to mitosis onset. Red arrowhead indicates pre-mitotic protrusive cell; yellow dot indicates mitotic cell; red dots indicates sister cells after division; and dotted white line indicates IPL. Scale bar: 5 μm. (D) Position and angle of HCpr mitosis is heterogenous. Yellow arrowheads indicate mitotic HCprs; white dots indicate sister HCs after division; white dotted line indicates OPL (top) and IPL (bottom). Scale bar: 10 μm. (D′) Percentage distribution of HCpr position of division. (E) Position (μm), (F) duration (min) and (G) angle of HCpr mitosis. (H,I) Frequency of mitotic (H) position and (I) duration. (J) Plot of mitotic duration versus position shows no strong correlation. Regression analysis was carried out using Pearson's correlation (r).

similar mitotic positioning pattern (Fig. S1E). Only in very rare cases did HCprs divide in the RGC layer (Fig. S2A). Frequency analysis confirmed a bias towards OPL positions as 41% of HCpr

divisions occurred close to the OPL (distance=0-6 μm), whereas the remaining 59% spread along the INL (Fig. 1D′,E,H). This suggests that HCprs favour divisions closer to the prospective HC layer.

Although this bias has not been shown previously, it was postulated that divisions close to the OPL facilitate rapid synaptic contacts between HCs and their partners (Godinho et al., 2007).

To understand whether these positional differences were connected to differences in HCpr mitotic behaviour, we analysed the duration of mitosis from rounding to anaphase onset (Fig. 1C,F). Single cell and frequency distribution analysis (n=404, N=20) revealed that while 62% of HCprs divided within the first 30 min after rounding, mitosis length varied from 10 min to 260 min (Fig. 1F,I). This is markedly different from what has been reported for retinal progenitor cells that have very reproducible mitotic timing lasting 25±3 min (Leung et al., 2011). To reveal potential differences between cells with short versus long mitotic length, we used a nuclear marker to differentiate between chromatin condensation, metaphase plate formation and DNA segregation. We found that the time between metaphase and anaphase was similarly diverse as overall mitotic length (Fig. S2B). Cells that took longer between metaphase plate formation and final division showed intense spindle rocking before anaphase onset (Fig. S2C, Movie 2). Moreover, final division angles showed a wide distribution variety (n=377, N=21) (Fig. 1D,G), suggesting that HCprs can divide with any directionality. Nevertheless, a bias towards 0° and 90° division angles was seen. No strong correlations were observed between division angle and timing of spindle positioning (Fig. S2D,E). In addition, the position of mitotic cells showed no strong connection to mitotic length (Fig. 1J), suggesting that duration of spindle positioning was the main factor in mitotic length distribution. Together, our data shows that division position, duration of final mitosis and spindle orientation are not stereotypical but vary widely among HCprs. However, independently of these variations, the resulting HCs consistently reach their correct layer (Fig. 1B, Movie 1).

HCprs exhibit heterogenous cell cycle timing

The fact that divisions of HCprs can, in principle, occur at any position within the INL made us ask whether these cells follow an intrinsic cell cycle timer that is responsible for cell divisions occurring independently of HCpr position. To test this idea, we tracked HCprs from apical birth to final division (n=23, N=10) (Fig. 2A, Movie 3). Cell cycle duration ranged from 11 h 15 min to 16 h 41 min, with an average of 13 h (Fig. 2C). Therefore, HCpr cycles were much longer than those reported for progenitor cells, which, albeit varied, have an average cell cycle length of 7.3 h at 30 hpf and 5.3 h at 42 hpf (Matejčić et al., 2018). As we used light sheet microscopy to analyse cell cycle timing, it is unlikely that differences were due to increased phototoxicity (Icha et al., 2016, 2017). No clear correlation between cell cycle length and distance from apical surface during division was seen (Fig. 2D).

Studies of fixed chick retinae suggested that HCprs undergo S phase during apical-basal migration and arrest in G2 while stalling in the INL (Boije et al., 2009). We tested this notion using PCNA (proliferating cell nuclear antigen) as a marker to unambiguously follow HCpr cell cycle phases (Leung et al., 2011) (Fig. 2A,B, Movie 3). Interestingly, we found that HCprs passed G1 and S phase at diverse positions along the INL (Fig. 2B). Cell were seen in G1 in the INL when HCprs are already multipolar. In addition, HCprs could be in S phase during basal as well as apical migration (Fig. 2B). In addition, we found that G2 [defined as time between disappearance of PCNA dots and cell rounding (Leung et al., 2011)] covered a rather short span of the overall cell cycle length (Fig. 2E) often occurring close to the OPL (Fig. 2B).

Together, these data make it unlikely that HCprs arrest in G2 before apical migration in zebrafish. Furthermore, our results argue against an intrinsic cell cycle timer responsible for mitotic onset (Fig. 2).

HC migration is non-stereotypic and varies in length and overall trajectories

It has previously been reported that maturing HCs undergo bidirectional migration before final lamination (Chow et al., 2015; Edqvist and Hallböök, 2004; Weber et al., 2014). However, so far only small cohorts of cells have been analysed using confocal microscopy with time resolution of 15 min or longer and focusing on different movement phases (Chow et al., 2015). To understand the stereotypicity of HC single cell migration, we followed cells from birth to final positioning using light sheet microscopy at 5 min intervals (from here on we will use the term HC for all migration behaviour before and after final division) (n=21 cells N=11) (Fig. 3A, Movie 4). The timing between birth and final positioning of HCs varied, broadly spanning between 9 h and almost 16 h (Fig. 3B). In addition, timing between birth, retraction of the apical process and final position varied (Fig. S3B). Single cell trajectory analysis revealed that, in contrast to the highly stereotypic migration behaviour of RGCs (Icha et al., 2016), each HC followed its own individual path and migration tracks took varying amounts of time (Fig. 3C, Fig. S3A). Trajectories are faster and more directed at early migration stages, as verified by mean square displacement and directionality analysis (Fig. 3C,D, Fig. S3C), most likely due to the maintenance of HC apical attachment (Chow et al., 2015). However, trajectories become more diverse and less directed after this stage (Fig. 3C,D, Fig. S3C). Tangential migration differed significantly among HCs, showing some cells are more constrained in nasal-temporal direction and others moving substantially along this axis (Fig. 3E). Despite these single cell differences, all HCs robustly reached their correct layer where they start polarizing (Fig. 3A, Movie 4).

HCs always migrate into the AC layer before apical turning and the depth of this migration depends on the presence of the IPL

Similar to other parameters, the depth of migration also varied strongly among individual HCs (Fig. 3C,F, Fig. S3). To find tissue-wide parameters responsible for these differences, we analysed how migration depth correlates with the formation of the IPL, which starts around 54 hpf and contains processes connecting amacrine cells (ACs), BCs and RGCs (Godinho et al., 2005). When defining the distance between the final OPL and IPL as 100% of the migratory path, shallow cells reached less than 50% of this distance, while HCs moving more deeply could surpass the prospective IPL position by 20% (Fig. 3F,G). However, HC migration deeper than the prospective IPL occurred only before this structure emerged (Fig. 3G,H). Early HCs that pass the depth of the prospective IPL were able to return to apical positions (Fig. 3H). Once the IPL was formed, however, HCs did not migrate below it (Fig. 3G,H). Interestingly, regardless of migration depth, all HCs were in contact with the AC layer (Fig. 3H and Movie 1), suggesting that migration into the AC layer is necessary for returning apically. As HCs cannot go deeper than the IPL after its formation, this structure most likely acts as a steric hindrance for HCs.

HC sister cell dispersal varies in time and in final nasal-temporal cell distance

Despite the variations found for HC cell cycle and migration parameters, HC layer formation occurred robustly in all embryos imaged (N=21). We therefore speculated that sister cell dispersal is important to fill the HC layer independently of single cell behaviour. We thus expected that this dispersal showed similar heterogeneity as other parameters to buffer the previous cell cycle variability and
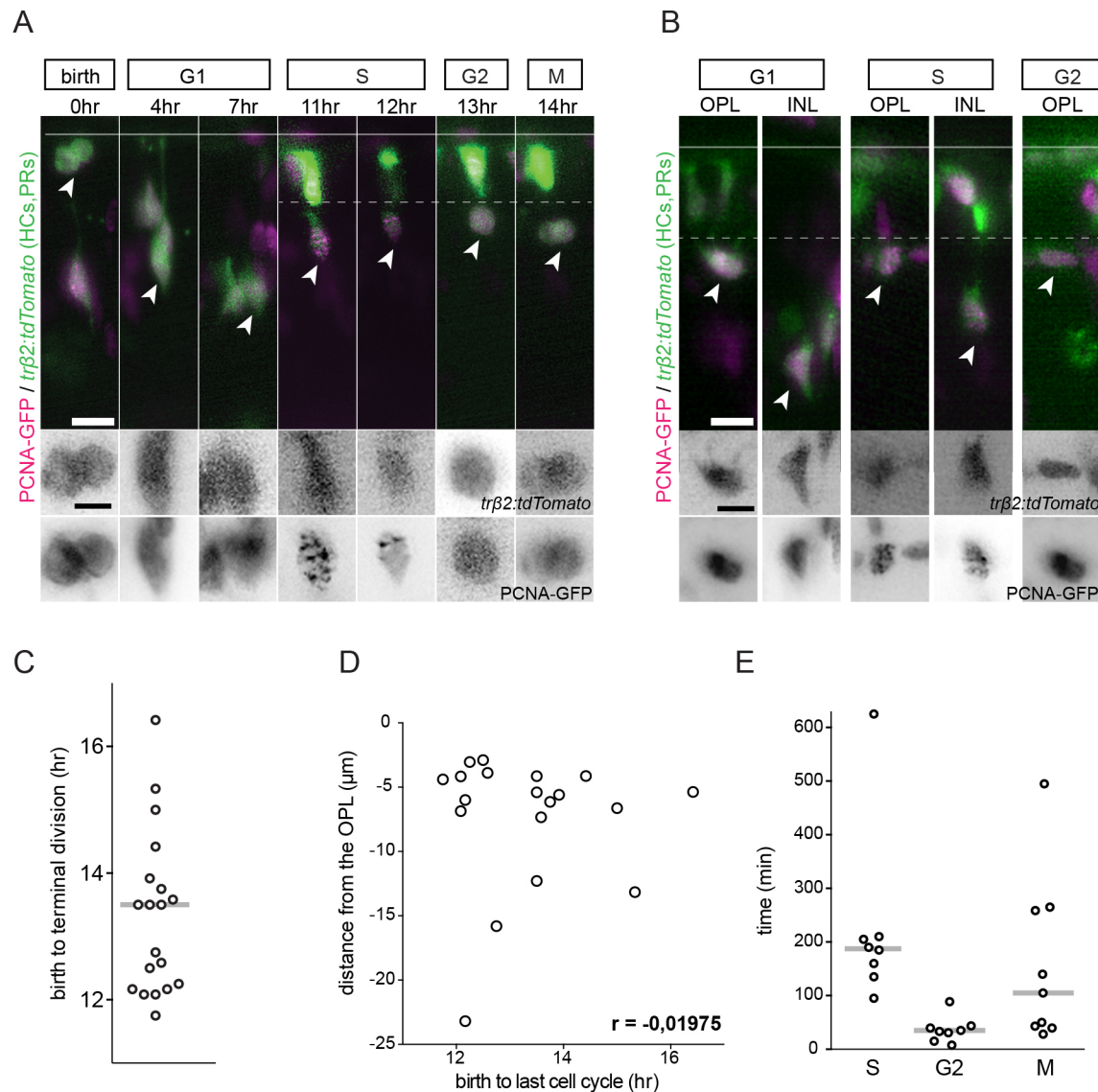
Fig. 2. HCprs undergo long heterogenous cell cycles. (A) Montage of the HCpr cell cycle. *Trβ2:tdTomato* (HCpr, green) and PCNA-GFP (nuclei, magenta). White arrowheads indicate the tracked cell. The OPL is indicated by a dotted white line. Scale bar: 10 μm. Bottom panels show *Trβ2:tdTomato* and PCNA-GFP individually. Scale bar: 5 μm. (B) HCpr cell cycle phases occur at different positions in the INL. *Trβ2:tdTomato* (HCpr, green) and PCNA-GFP (nuclei, magenta) are shown. White arrowheads indicate the cell that was followed. The OPL is indicated by a dotted white line. Scale bar: 10 μm. Bottom panels show *Trβ2:tdTomato* and PCNA-GFP individually. Scale bar: 5 μm. (C) Distribution of HCpr cell cycle length. Line indicates the mean. (D) Scatter plot of HCpr cell cycle length versus HCpr position shows a lack of strong dependence. Regression analysis was carried out using Pearson correlation (r). (E) Distribution of HCpr cell cycle phase lengths: S, G2 and M. Lines indicate the means.

stochastic migration patterns observed. This was indeed the case (*n*=20, *N*=6). Although some sister HCs moved substantially in apicobasal direction after terminal divisions and ended up in close nasal-temporal vicinity (Fig. 4A,B and Movie 5), others moved very little in the apicobasal direction but dispersed much more laterally with final positions of sister cell bodies one-tenth of a micrometer apart (Fig. 4C,D). Lateral HC sister cell movement took between 1 h 40 min and 6 h 30 min (Fig. 4E), and lateral dispersion differed substantially among cohorts of sister cells upon final mitosis, ranging from 0.6 μm to 29 μm (Fig. 4F).

Thus, like other parameters, sister cell dispersion within the HC layer is highly heterogeneous. Interestingly, sister HCs can end up far apart from each other, arguing against the idea that functional retinal columns exist, at least when it comes to HC clones (He et al., 2012), as suggested previously for mouse horizontal cells (Reese et al., 1995).

DISCUSSION
Overall, the use of long-term quantitative light sheet microscopy enabled us to present first evidence that, in addition to stochasticity in retinal fate decisions (Baye and Link, 2007; Del Bene et al., 2008; He et al., 2012), later stages of retinal development, in particular retinal laminations, also show high degrees of variability. The example presented here, the formation of the HC layer, demonstrates this to an extreme extent: all parameters analysed over hundreds of cells from many embryos showed heterogeneity. The term stochasticity applies, as single cell behaviour cannot be predicted. Instead, some degree of random chance seems to govern division timing and position and particularly the migratory path of the cells. Our findings are summarized in Fig. 4G.

At this point, we cannot completely exclude the possibility that common parameters could be found in different subsets of
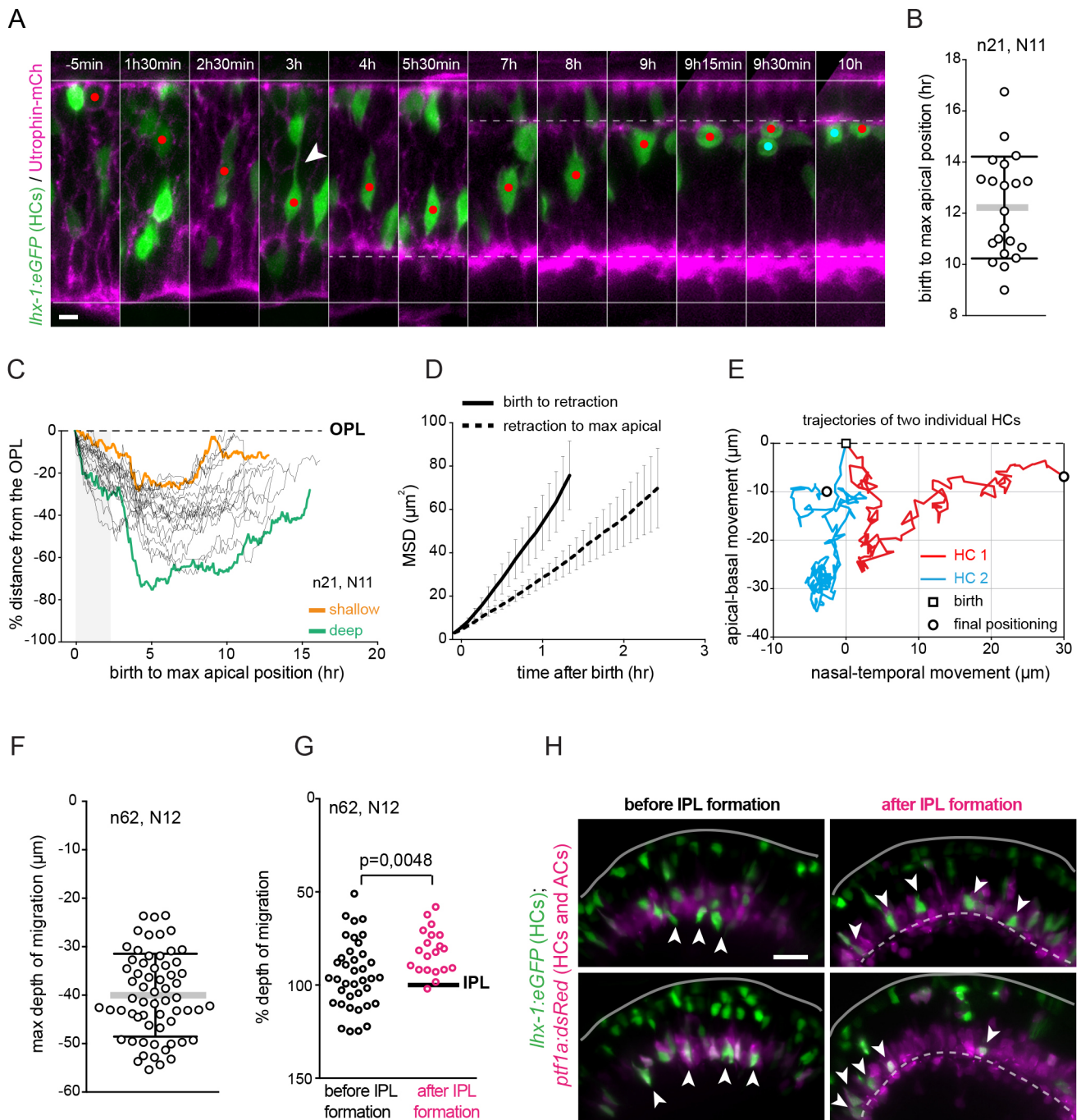
4

Fig. 3. Bi-directional HC migration is heterogenous but HCprs always stopover within the amacrine cell layer and heterogeneity in HC depth depends on IPL formation. (A) Montage of HC migration from HCpr birth to final positioning. *lhx-1:eGFP* (HC and PR, green) and *Utrophin-mCherry* (cell outline, magenta). Red dot indicates tracked cell; white arrowhead indicates apical process before detachment; red and cyan dots indicate sister HCs after terminal division. Time is relative to HC birth. White lines indicate apical surface (top) and basal membrane (bottom). White dotted lines indicate OPL (top) and IPL (bottom). Scale bar: 5 µm. (B) Scatter plot of HC birth to max apical position. Data are mean±s.d. (C) Single cell trajectories of HC bidirectional migration from birth to final positioning as a percentage of the total thickness of the retina. The orange and green lines provide examples of a shallow and a deep track, respectively. The shadow indicates the initial stage of migration. (D) Mean square displacements±s.d. of HC for different phases; from birth to apical process retraction (solid line) from retraction to final positioning (dashed line). (E) Representative examples of HC migration along the apical-basal and nasal-temporal retinal axis. (F) Distribution of HC maximum migration depth. Data are mean±s.d. with individual data points indicated. (G) Percentage of HC maximum migration depth relative to the retinal thickness, before (black circles) and after (magenta circles) IPL (black line) formation. (H) Examples of HC migration before and after IPL formation. *lhx-1:eGFP* (HC and PRs, green) and *ptf1a:dsRed* (ACs and HCs, magenta). Solid and dashed white lines indicate apical surface and IPL, respectively. White arrowheads indicate HC position. Scale bar: 10 µm.

HCs due to the lack of subset-specific live imaging markers. However, the broad spread of our data argues against this possibility. To resolve this point, single cell sequencing of HCs would be an attractive possibility. Owing to the scarcity of HCs within the retinal cell population, however, this might be a demanding task.
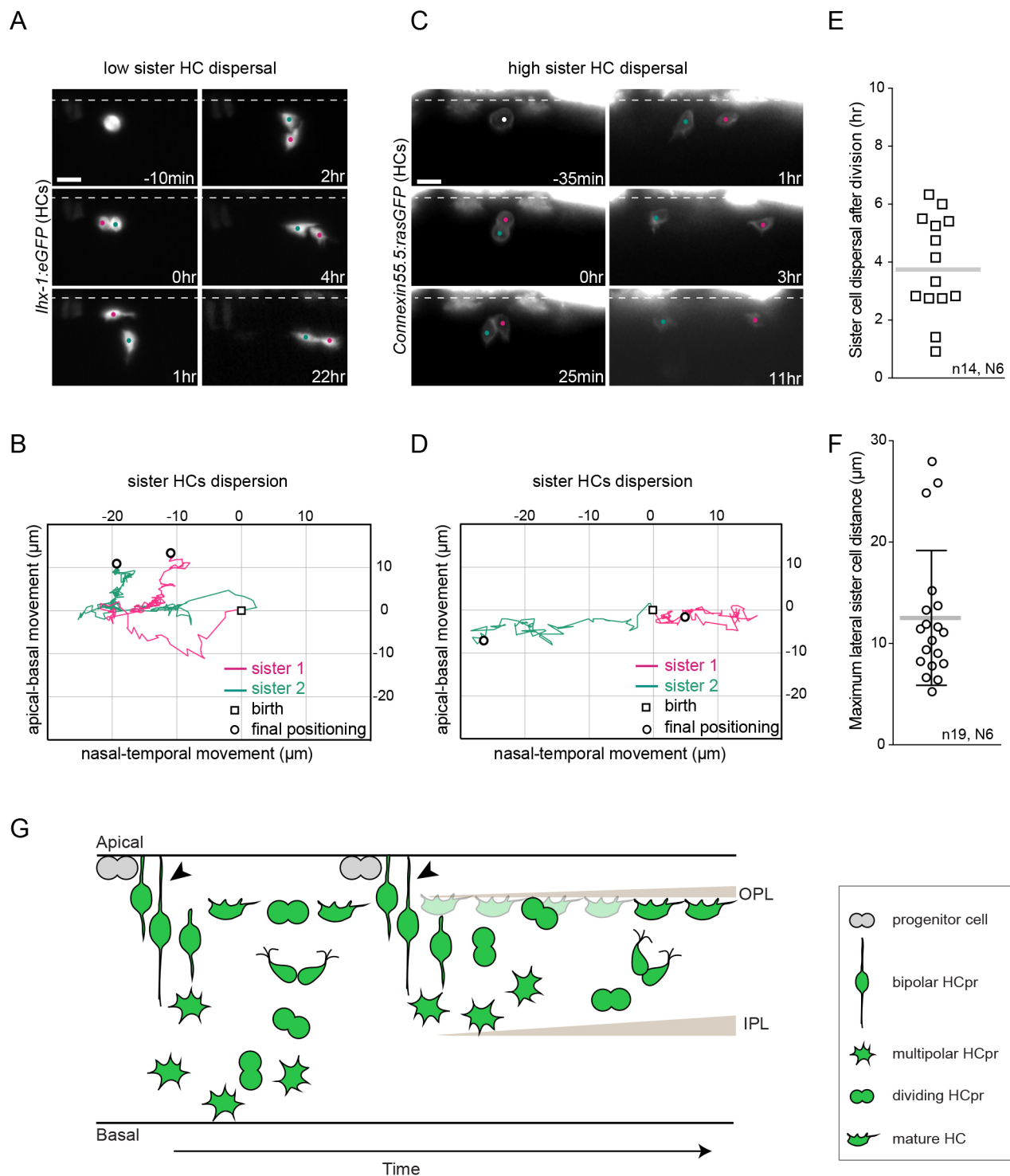
Fig. 4. Sister cell dispersal is heterogenous in length and distance between cells. (A) Example of sister cell dispersal in *lhx-1:eGFP*. Scale bar: 10 µm. (B) Trajectories of A. (C) Example of sister cell dispersal in *Connexin:rasGFP*. Scale bar: 10 µm. (D) Trajectories of C. (E) Duration of HC sister cell dispersion. Line indicates the mean. (F) Maximum lateral distance between sister cells upon final HC mitosis. Data are mean±s.d. (G) Scheme of HC mitotic and migration behaviour. Retinal progenitors (grey) generate HCprs (green) apically. HCprs first migrate basally while keeping their apical attachment (black arrowheads). Upon losing this attachment, HCprs undergo multipolar migration, reaching the basal INL. Depth of basal migration depends on IPL presence (no IPL indicates deep migration; presence of IPL indicates shallow migration). HCprs invert movement and freely migrate apically to form the HC layer. En route, HCprs undergo a terminal mitosis along the INL.

Other cell types that laminate in the vertebrate retina show much more stereotypic behaviour than HCs. RGCs laminate via somal translocation, and their timing and migration trajectories are highly stereotypic (Icha et al., 2016). What could be the reason for these differences? We speculate that one cause could be the presence or absence of an apical cell attachment. RGCs are apically attached until they reach the RGC layer and only upon apical process detachment do they undergo random walk-like behaviour during

fine positioning (Icha et al., 2016). HCs instead lose their apical attachment early during migration (Chow et al., 2015) (Fig. 4G) and from then on navigate freely through the tissue without any predisposed track information. Thus, timing and depth of migration can vary and this heterogeneity needs to be buffered by the heterogeneity of other parameters such as sister cell dispersal. Together, this ensures robust HC layer formation despite single parameter variability. Consequently, although the behaviour of single cells is not predictable, at the tissue level it still produces a robust pattern. The obvious next steps will be to understand how this emergence of a well-organized tissue from seemingly chaotic single cell behaviour is ensured. To achieve this, it is necessary to extract the tissue-wide parameters guiding it. Such parameters could be coded in chemical guidance cues; however, mechanical tissue properties could also play a role. Follow up studies will therefore raise an exciting new array of questions, such as which additional neuronal pattern formation phenomena involve variability of the cell cycle, the positioning parameters and stochastic migration patterns, and how this single cell variability forms reproducible lamination at the tissue level.

MATERIALS AND METHODS

Horizontal cell labelling

HCs have been identified in vertebrate retinas from fish to humans and are divided into two main types: axon bearing and axon less. In the adult zebrafish retina, three types of axon-bearing HCs (H1, H2 and H3) and one type of axon-less HC (HB) have been identified (Song et al., 2008). HCs can be labelled for different proteins and transcription factors (TFs) that are often expressed in a subtype-specific manner (Fig. S1A). In zebrafish, the gap junction protein connexin55.5 is expressed in HCs. Although some studies propose that this marker is predominantly expressed in HA types of HCs (Godinho et al., 2007; Shields et al., 2007), a more recent study suggests that it is expressed in more diverse subtypes (Klaassen et al., 2016). The pancreas-specific transcription factor 1a (Ptf1a) is expressed in all HC subtypes in the zebrafish retina (Jusuf et al., 2011), while the TF thyroid hormone receptor β2 (trβ2) labels 70% of Ptf1a-positive HCs in the zebrafish retina (Suzuki et al., 2013). In the chick retina, the Lim family TFs Islet1 (Isl1) and Lim1/Lhx1 are expressed in axon-less and axon-bearing HC subtypes, respectively (Edqvist et al., 2008). Whether Lim1/Lhx1 has a similar heterogenous expression pattern in HC subtypes in zebrafish is not currently known but we see that the majority of Ptf1a-positive HCs are labelled by this marker. Here, we use a combination of these HC markers (Fig. S1B,C), and show that no marker-specific HC behaviour is observed (Fig. S1E).

Zebrafish work

Zebrafish were maintained and bred at 26.5°C. Zebrafish embryos were raised at 28.5°C or 32°C and staged in hours post fertilization (hpf) according to Kimmel et al. (1995). Embryos were kept in E3 medium, which was supplemented by 0.003% 1-phenyl-2-thiourea (PTU) from 8±1 hpf onwards and renewed daily. PTU was added to prevent pigmentation. Embryos were anesthetized in 0.04% tricane methanesulfonate (MS-222; Sigma-Aldrich) prior to sorting for fluorescent signal (>35 hpf). Refer to Table S1 for a list of transgene lines used in this study. See Table S3 for a list of experiments, and numbers of cells and embryos. All animal work was performed in accordance with the European Union (EU) directive 2010/63/EU, as well as the German Animal Welfare act.

DNA injections

To mosaically label HCs, DNA constructs were injected into the cytoplasm of one-cell stage embryos. Constructs were diluted in double-distilled H_2O supplemented with 0.05% Phenol Red (to visualize the injection material) (Sigma-Aldrich). Injected volumes ranged from 1 to 1.5 nl. DNA concentrations were 20-30 ng/μl and did not exceed 30 ng/μl even when multiple constructs were injected. See Table S2 for a list of injected constructs.

Heat shock of embryos

To induce expression of heat shock promoter (hsp70)-driven constructs and transgenes, embryos were incubated in a water bath 1.5-3 h before imaging for 20 min at 39°C. See Tables S1 and S2 for a list of heat-shock induced transgenes and constructs, respectively.

Blastomere transplantations

Transplantation dishes were prepared by floating a plastic template in a Petri dish that was half-filled with 1% low-melting-point agarose in E3. When the agarose solidified, plastic templates were gently removed, leaving an agar mould that contained rows of wells to hold embryos. Embryos at stages high to sphere were dechorionated in pronase (Roche) and dissolved in Danieu's buffer. Dechorionated embryos were transferred to wells in agarose moulds using a wide-bore fire-polished glass pipet. At the 1000-cell stage, cells from the donor embryos were transplanted into the animal pole of the acceptor embryos using a Hamilton syringe. The animal-pole region is fated to become retina and forebrain tissue. Transplanted embryos were kept on agarose for about 3-5 h and then transferred onto glass dishes that contained E3 medium supplemented with 0.003% PTU and antibiotics (100 U of penicillin and streptomycin, Thermo Fisher Scientific). Transplanted embryos were identified via fluorescence and imaged from 42 hpf (see Table S3).

In vivo light sheet fluorescent imaging (LSFM)

Imaging started between 35 hpf and 48 hpf (see Table S3). Embryos were manually dechorionated and mounted in glass capillaries in 1% low-melting-point agarose as previously described (Icha et al., 2016). The sample chamber was filled with E3 medium containing 0.01% MS-222 (Sigma-Aldrich) (to immobilize embryos) and 0.2 mM PTU (Sigma-Aldrich). Imaging was performed on a Zeiss Light sheet Z.1 microscope with a Zeiss Plan-Apochromat 20× water-dipping objective (NA 1.0) at 28.5°C. Z-stacks spanning the entire eye (100-120 μm) were recorded with 1 μm optical sectioning. Z-stacks were recorded every 5 min for 6-42 h, with double-sided illumination mode. The system was operated by the ZEN 2014 software (black edition).

Image processing and analysis

The raw LSFM data were deconvolved in ZEN 2014 software (black edition, release version 9.0) using the Nearest Neighbour algorithm. Minimal image pre-processing was implemented prior to image analysis, using open source ImageJ/Fiji software (fiji.sc). Processing consisted of extracting image subsets or maximum intensity projections of a few slices. Processed files were then analysed in Fiji and the data were plotted using MATLAB or Microsoft Excel.

Mitosis and cell cycle length analysis

Mitosis length analysis

HC rounding was defined as the onset of mitosis and the point of anaphase as the end of mitosis. The time required for this was defined as the mitosis length (Fig. 1C,F).

Metaphase-to-anaphase length

To visualize HC nuclei, Tg(lhx-1:eGFP) animals were crossed with Tg(hsp70:H2B-RFP) animals. Metaphase was detected by the condensed and elongated nature of the chromatin in the centre of the cell. Anaphase was assessed by chromatin separation (Fig. S2C).

HC cell cycle period

To assess cell cycle phase of HCs, the Hsp70::EGFP-PCNA DNA plasmid was injected into one-cell stage embryos. Individual PCNA[+] HCs were manually followed in Fiji from birth to terminal mitosis. Onset of G1 was defined as the time of HC birth at the apical side. The end of G1 was defined as last timepoint prior to PCNA foci appearance (Fig. 2A). S phase was defined between the appearance and disappearance of PCNA foci (Fig. 2A). G2 was measured from the disappearance of PCNA foci (end of S phase) to cell rounding (Leung et al., 2011).

Division orientation

Division orientation was analysed manually using the angle tool in Fiji RRID:SCR_002285 (Schindelin et al., 2012) from maximum intensity

projections of five slices of LSFM images. For each observed anaphase cell, a line was drawn parallel to the division plane, and the angle was measured with respect to the temporal-nasal tissue axis (horizontal image axis) (Fig. S1D). Data were plotted as a polar histogram in MATLAB.

Mitotic position
The Fiji Line tool was used to manually measure the distance from the centre of the mitotic HCpr (at rounding) and the OPL in the maximum projection of three to five consecutive z slices (Fig. S1D).

Sample drift correction
First, maximum projected sub-stacks (five z slices) of the raw live images were generated in Fiji. xy-drift of 2D stacks was then corrected using a manual drift correction Fiji plug-in (imagej.net/Manual_drift_correction_plugin).

Analysis of HC bidirectional migration, directionality ratio and mean square displacement analysis
Labelling migrating HCs
Three approaches were used to label HCs: (1) double transgenic animals were generated by crossing transgene lines in Table S1 [*Tg(lhx-1:eGFP);Tg(ath5: gap-RFP),Tg(lhx-1:eGFP);Tg(*actb2*:mCherry-Hsa.UTRN)* and *Tg(lhx-1: eGFP); Tg(ptf1a:DsRed)* (Table S3)]; (2) blastomere transplantation was performed to mosaically label HCs; and (3) microinjection of plasmid DNA encoding *trβ2:tdTomato* or *Connexin:55.5:ras*GFP was used to mosaically label HCs in the retina (Tables S2 and S3).

Tracking migrating HCs
The migrating HCs were manually tracked by following the centre of the cell body in 2D images using MTrackJ plug-in in Fiji (Meijering et al., 2012). The resulting trajectories were analysed as described previously (Icha et al., 2016). Mean square displacements and directionality ratios were calculated using the DiPer program (Gorelik and Gautreau, 2014) and executed as a macro in Excel (Microsoft).

Maximum depth of HC migration analysis
The relative percentage of maximum HC depth was defined by the apex of HC basal position using individual HC trajectories. At this point, the distance of the centre of the cell body from the OPL was divided by the OPL to IPL thickness (Fig. S1F).

Statistical analysis
All statistical analysis was performed using Prism software (version 6.0c for Mac OS; GraphPad Software) to create graphs. In total, data were collected from 432 HCs in 24 independent time-lapse imaging experiments (Table S3). Pearson correlation coefficient was used to examine associations between length, position and angle of HCpr mitosis as well as HCpr cell cycle length and position. The correlation coefficient, r, ranges from −1 to +1, where 1 indicates perfect correlation, 0 to 1 indicates the two variables tend to increase or decrease together, 0 indicates that the two variables do not vary together at all, −1 to 0 indicates that one variable increases as the other decreases and −1 indicates perfect negative or inverse correlation.

Author contributions
Conceptualization: R.A., C.N.; Methodology: R.A., A.A.L., C.N.; Validation: R.A., A.A.L.; Formal analysis: R.A., A.A.L.; Investigation: R.A., A.A.L., C.N.; Resources: C.N.; Data curation: R.A.; Writing - original draft: R.A., C.N.; Visualization: R.A.; Supervision: R.A., C.N.; Project administration: C.N.; Funding acquisition: R.A., C.N.

Supplementary information
Supplementary information available online at
http://dev.biologists.org/lookup/doi/10.1242/dev.173450.supplemental

References
Amini, A., Rocha-Martins, M. and Norden, C. (2018). Neuronal migration and lamination in the vertebrate retina. *Front. Neurosci.* **11**, 742. doi:10.3389/fnins. 2017.00742

Baye, L. M. and Link, B. A. (2007). Interkinetic nuclear migration and the selection of neurogenic cell divisions during vertebrate retinogenesis. *J. Neurosci.* **27**, 10143-10152. doi:10.1523/JNEUROSCI.2754-07.2007

Boije, H., Edqvist, P.-H. D. and Hallböök, F. (2009). Horizontal cell progenitors arrest in G2-phase and undergo terminal mitosis on the vitreal side of the chick retina. *Dev. Biol.* **330**, 105-113. doi:10.1016/j.ydbio.2009.03.013

Chow, R. W.-Y., Almeida, A. D., Randlett, O., Norden, C. and Harris, W. A. (2015). Inhibitory neuron migration and IPL formation in the developing zebrafish retina. *Development* **142**, 2665-2677. doi:10.1242/dev.122473

Del Bene, F., Wehman, A. M., Link, B. A. and Baier, H. (2008). Regulation of neurogenesis by interkinetic nuclear migration through an apical-basal notch gradient. *Cell* **134**, 1055-1065. doi:10.1016/j.cell.2008.07.017

Edqvist, P.-H. D. and Hallböök, F. (2004). Newborn horizontal cells migrate bi-directionally across the neuroepithelium during retinal development. *Development* **131**, 1343-1351. doi:10.1242/dev.01018

Edqvist, P.-H. D., Lek, M., Boije, H., Lindbäck, S. M. and Hallböök, F. (2008). Axon-bearing and axon-less horizontal cell subtypes are generated consecutively during chick retinal development from progenitors that are sensitive to follistatin. *BMC Dev. Biol.* **8**, 46. doi:10.1186/1471-213X-8-46

Godinho, L., Mumm, J. S., Williams, P. R., Schroeter, E. H., Koerber, A., Park, S. W., Leach, S. D. and Wong, R. O. L. (2005). Targeting of amacrine cell neurites to appropriate synaptic laminae in the developing zebrafish retina. *Development* **132**, 5069-5079. doi:10.1242/dev.02075

Godinho, L., Williams, P. R., Claassen, Y., Provost, E., Leach, S. D., Kamermans, M. and Wong, R. O. L. (2007). Nonapical symmetric divisions underlie horizontal cell layer formation in the developing retina in vivo. *Neuron* **56**, 597-603. doi:10.1016/j.neuron.2007.09.036

Gorelik, R. and Gautreau, A. (2014). Quantitative and unbiased analysis of directional persistence in cell migration. *Nat. Protoc.* **9**, 1931-1943. doi:10.1038/ nprot.2014.131

He, J., Zhang, G., Almeida, A. D., Cayouette, M., Simons, B. D. and Harris, W. A. (2012). How Variable Clones Build an Invariant Retina. *Neuron* **75**, 786-798. doi:10.1016/j.neuron.2012.06.033

Icha, J., Kunath, C., Rocha-Martins, M. and Norden, C. (2016). Independent modes of ganglion cell translocation ensure correct lamination of the zebrafish retina. *J. Cell Biol.* **215**, 259-275. doi:10.1083/jcb.201604095

Icha, J., Weber, M., Waters, J. C. and Norden, C. (2017). Phototoxicity in live fluorescence microscopy, and how to avoid it. *BioEssays* **39**, 1700003-15. doi:10. 1002/bies.201700003

Jusuf, P. R., Almeida, A. D., Randlett, O., Joubin, K., Poggi, L. and Harris, W. A. (2011). Origin and determination of inhibitory cell lineages in the vertebrate retina. *J. Neurosci.* **31**, 2549-2562. doi:10.1523/JNEUROSCI.4713-10.2011

Kimmel, C. B., Ballard, W. W., Kimmel, S. R., Ullmann, B. and Schilling, T. F. (1995). Stages of embryonic development of the zebrafish. *Dev. Dyn.* **203**, 253-310. doi:10.1002/aja.1002030302

Klaassen, L. J., de Graaff, W., Van Asselt, J. B., Klooster, J. and Kamermans, M. (2016). Specific connectivity between photoreceptors and horizontal cells in the zebrafish retina. *J. Neurophysiol.* **116**, 2799-2814. doi:10.1152/jn.00449. 2016

Leung, L., Klopper, A. V., Grill, S. W., Harris, W. A. and Norden, C. (2011). Apical migration of nuclei during G2 is a prerequisite for all nuclear motion in zebrafish neuroepithelia. *Development* **138**, 5003-5013. doi:10.1242/dev.071522

Matejčić, M., Salbreux, G. and Norden, C. (2018). A non-cell-autonomous actin redistribution enables isotropic retinal growth. *PLoS Biol.* **16**, e2006018. doi:10. 1371/journal.pbio.2006018

Meijering, E., Dzyubachyk, O. and Smal, I. (2012). Methods for cell and particle tracking. *Meth. Enzymol.* **504**, 183-200. doi:10.1016/B978-0-12-391857-4.00009-4

Reese, B. E., Harvey, A. R. and Tan, S. S. (1995). Radial and tangential dispersion patterns in the mouse retina are cell-class specific. *Proc. Natl. Acad. Sci. U.S.A.* **92**, 2494-2498. doi:10.1073/pnas.92.7.2494

Schindelin, J., Arganda-Carreras, I., Frise, E., Kaynig, V., Longair, M., Pietzsch, T., Preibisch, S., Rueden, C., Saalfeld, S., Schmid, B. et al. (2012). Fiji: an open-source platform for biological-image analysis. *Nat. Methods* **9**, 676-682. doi:10.1038/nmeth.2019

DEVELOPMENT

Shields, C. R., Klooster, J., Claassen, Y., Ul-Hussain, M., Zoidl, G., Dermietzel, R. and Kamermans, M. (2007). Retinal horizontal cell-specific promoter activity and protein expression of zebrafish connexin 52.6 and connexin 55.5. *J. Comp. Neurol.* **501**, 765-779. doi:10.1002/cne.21282

Song, P. I., Matsui, J. I. and Dowling, J. E. (2008). Morphological types and connectivity of horizontal cells found in the adult zebrafish (Danio rerio) retina. *J. Comp. Neurol.* **506**, 328-338. doi:10.1002/cne.21549

Suzuki, S. C., Bleckert, A., Williams, P. R. Takechi, M., Kawamura, S. and Wong, R. O. (2013). Cone photoreceptor types in zebrafish are generated by symmetric terminal divisions of dedicated precursors. *Proc. Natl. Acad. Sci. USA* **110**, 15109-15114. doi:10.1073/pnas.1303551110

Weber, I. P., Ramos, A. P., Strzyz, P. J., Leung, L. C., Young, S. and Norden, C. (2014). Mitotic position and morphology of committed precursor cells in the zebrafish retina adapt to architectural changes upon tissue maturation. *Cell Rep.* **7**, 386-397. doi:10.1016/j.celrep.2014.03.014

DEVELOPMENT